ROYAL SOCIETY
OF CHEMISTRY

Hydroflux-assisted cold sintering: eutectic mixtures for boosting ionic conductivity in LATP solid-state electrolytes†

Andrés Mormeneo-Segarra, [ID] [ab] Sergio Ferrer-Nicomedes, [ID] [ab] Nuria Vicente-Agut [ID] *[ab] and Antonio Barba-Juan [ID] [ab]

Superior electrical properties have been achieved for a $Li_{1.3}Al_{0.3}Ti_{1.7}(PO_4)_3$ (LATP) solid-state electrolyte (SSE) by using the novel hydroflux-assisted cold sintering process (HACSP) at 400 MPa, 200 °C and 90 minutes of sintering time. The use of the eutectic $LiOH:LiNO_3$ mixture, with 20 wt% content, as an hydroflux to assist the CSP has allowed to obtain a total ionic conductivity of 1.51×10^{-4} S cm^{-1} and an activation energy of 0.366 eV. Using water to better distribute the hydroflux along the LATP structure was found to be critical to the homogeneity and properties of the sample.

Introduction

Energy has become the key piece on the chessboard in recent years, which is why an efficient and environmentally friendly form of storage is required. Solid state batteries (SSBs) are the most likely candidates to meet the future efforts and challenges to come.[1–3] The use of solid state electrolytes (SSEs) in SSBs presents the greatest challenge in terms of design and performance, as they can prevent the growth of dendrites, providing greater stability to possible chemical reactions.[4] The SSEs studied so far have different structures,[5] of which NASICON is the most prominent. Among the materials with this type of structure, $Li_{1.3}Al_{0.3}Ti_{1.7}(PO_4)_3$ (LATP) stands out for its high total ionic conductivity ($\sim 10^{-3}$ S cm^{-1}) as well as its stability in the presence of ambient humidity.[6] In order to use SSEs in SSBs, the LATP powder has to be sintered. The method of sintering largely determines the properties of the final electrolyte, and the cost of manufacture. The cold sintering process (CSP) has emerged as a promising sintering technique to reduce the temperature and operating times, in contrast to conventional sintering techniques.[7,8] The CSP is based on reducing high sintering temperatures by using a transient liquid phase (TLP), a low temperature (below 350 °C) and a pressure of hundreds of MPa. Sintering takes place through a mass transfer mechanism called pressure solution creep based on the dissolution–precipitation of the material in the TLP: the material is dissolved in the outer surface of the particles and, after

evaporation of the TLP, it is precipitated at grain boundaries. The CSP has made it possible to obtain highly densified samples with excellent final physical properties.[9] Most of the studies in the literature on the CSP show that liquids at room temperature are used as a TLP, which evaporate at a temperature close to, but below the process temperature. However, the possibility of using hydrofluxes as a TLP has recently been tested, achieving good properties as shown in.

Table 1. In this case, a mixture of solid materials, that form an eutectic at sintering temperatures, acts as a TLP, remaining as a solid intergranular phase at room temperature.

Recently, Takashima *et al.*[10] have obtained cold-sintered samples of $Li_{1.5}Al_{0.5}Ge_{1.5}(PO_4)_3$ (LAGP) by using the mixture $LiNO_3:LiOH$ (60 : 40 mol%) as a hydroflux to assist the CSP. They obtained ionic conductivities ranging from 0.8×10^{-5} to 1.9×10^{-5} S cm^{-1} and a total activation energy of 0.42 ± 0.01 eV, concluding that the use of the hydroflux improved the electrical properties of the LAGP pellets because of the non-formation of the $AlPO_4$ layer at the grain boundaries.

To elucidate how this hydroflux affects the CSP of LATP powder and enhance its final properties, the authors prepared different LATP samples at ultra-low temperature with various hydroflux contents and found an optimum content of 20 wt% (with 5 wt% water as the homogenizing agent). The outstanding electrical properties obtained were a total ionic conductivity of 1.51×10^{-4} S cm^{-1} and an activation energy of 0.366 eV that are competitive with the ones obtained *via* conventional sintering at high temperatures.

Materials and methods

$Li_{1.3}Al_{0.3}Ti_{1.7}(PO_4)_3$ powder was prepared *via* a solid-state reaction as described in ref. 16 with a mean particle size of

[a] Department of Chemical Engineering, Universitat Jaume I, 12071, Castellón, Spain. E-mail: vicenten@uji.es
[b] Institute of Ceramic Technology, Universitat Jaume I, 12071, Castellón, Spain
† Electronic supplementary information (ESI) available. See DOI: https://doi.org/10.1039/d4ma00582a

Table 1 Materials obtained *via* the CSP using a hydroflux as a TLP

Material	Hydroflux	CSP conditions				Rel. density ϕ (%)	Ref.
		P (MPa)	T (°C)	t (min)	TLP		
LAGP	LiNO$_3$: LiOH (60 : 40 mol%)	400	220	300	18 (wt%)	88–92	10
ZnO	ZnO(OAc)$_2$·2H$_2$O	530	120	30	4	∼97	11
ZnO	NaOH : KOH (51 : 49 mol%)	90	200	30	5 + 5 of H$_2$O (vol%)	96	12
BaTiO$_3$	NaOH : KOH (50 : 50 mol%)	520	300	720	4–6 (wt%)	98–99	13
KNN	NaOH : KOH (50 : 50 mol%)	400	200	∼60	4–10 (vol%)	>92	14
KNN	NaOH : KOH (50 : 50 mol%)	400	200	120	10 (vol%)	93	15

0.415 μm. The hydroflux LiNO$_3$: LiOH (99 and 98% purity – Sigma Aldrich) was prepared by dissolving a mixture of LiNO$_3$ and LiOH in a molar ratio of 60 : 40 in distilled water to obtain good homogeneity. When complete dissolution was achieved, the mixture was dried in an oven at 100 °C. The dried mixture was mixed with a mortar and pestle to homogenize the resulting eutectic. A schematic view can be seen in Fig. 1(a).

Two different amounts of hydroflux, 15 and 20 wt% (higher levels lead to powder leakage from the mould), were added to the LATP powder with 5 wt% H$_2$O (15@H$_2$O and 20@H$_2$O samples) to improve the homogenization process of the LATP and the hydroflux, as shown in Fig. 1(b). Two other different samples were prepared without water as the homogenizing agent: one containing 20 wt% hydroflux (20@no-H$_2$O sample) and the other one simply by directly mixing the LiOH and LiNO$_3$ (without any previous treatment, 20@solids samples). Table 2 summarizes the four tested samples. The CSP experiments were carried out at 400 MPa, 200 °C and 90 minutes of dwell time, as these conditions allow the eutectic point of the hydroflux to be reached, as shown in Fig. 2, adapted from ref. 17, using an EQP-1 manual pellet press (EQUILAB). All sample's surface area equals 76.51 ± 0.01 mm^2. Densities were measured by mercury immersion, and the results are shown in Table S1 of the ESI† with the procedure description.
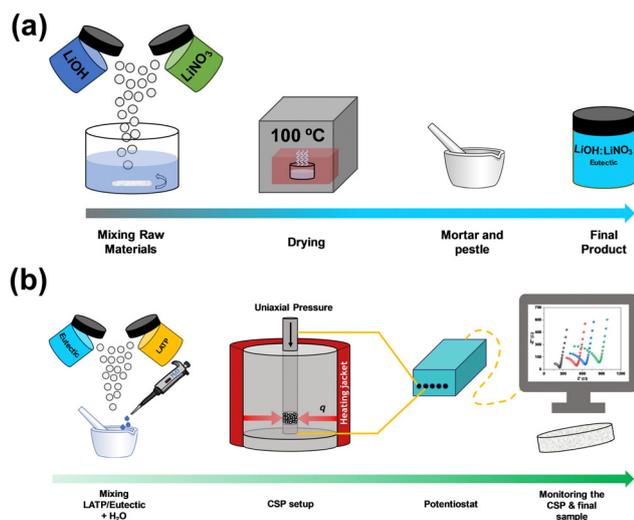
Table 2 Tested compositions for LATP sintering by the CSP using LiNO$_3$ and LiOH as the hydroflux in a molar ratio of 60 : 40

Hydroflux	TLP (wt%)	H$_2$O^a (wt%)	Sample
LiNO$_3$: LiOH	15	5	15@H$_2$O
	20	5	20@H$_2$O
	20	0	20@no-H$_2$O
LiNO$_3$ + LiOH	20	0	20@solids

^{a} Water is used only as a homogenizing agent (not as a TLP).

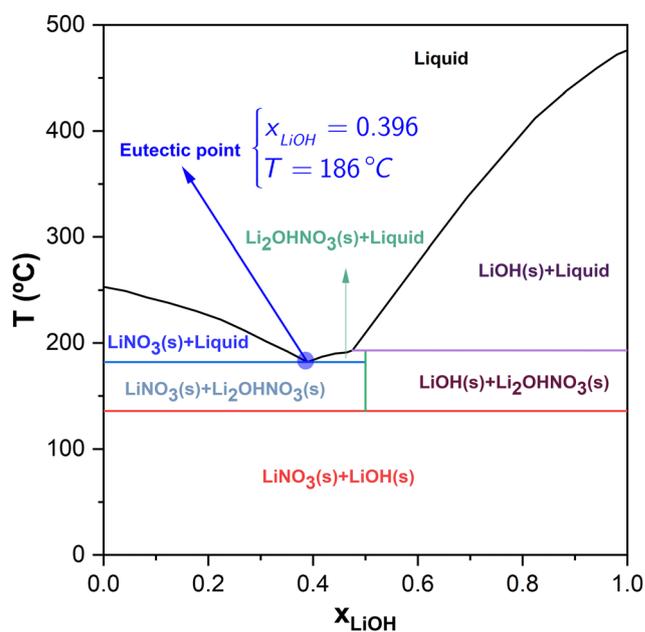**Fig. 2** Phase diagram of the LiOH:LiNO$_3$ mixture adapted from ref. 17.

Potentiostatic impedance measurements were carried out along the CSP using a Multi Autolab M204 potentiostat from AUTOLAB equipped with an impedance module FRA32 controlled by Nova 2.1 software. In the frequency range 1 MHz–50 Hz, and with a perturbation of 0.2 V, further experimental details can be found in the literature.[18,19] To fit the spectra, an equivalent circuit consisting of $(R_{tot}\text{CPE}_1)$ $(R_1\text{CPE}_2)\text{C}_1$ was used. R_{tot}, CPE$_1$, and $(R_1\text{CPE}_2)\text{C}_1$ represent the total resistance (sum of grain and grain-boundary), constant phase element and elements which fit impedance related to Li-ion diffusion within the electrolyte, respectively. Total
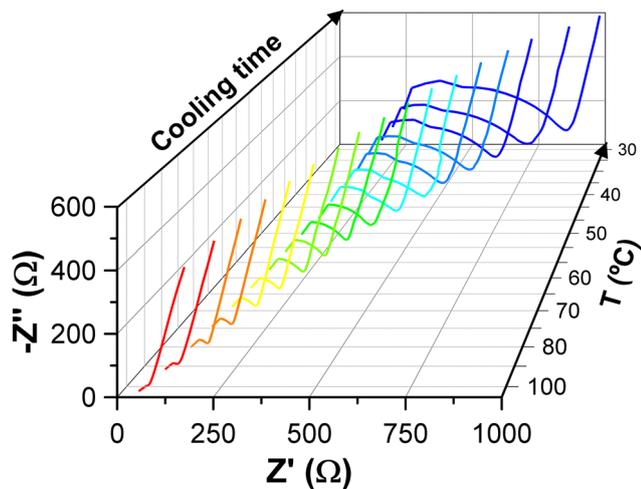

Fig. 1 (a) Preparation of eutectic mixtures. (b) CSP sample processing and *in operando* impedance measurements.

Fig. 3 Cooling impedance spectra of the 20@H₂O sample.

ionic conductivities, σ_{tot}, were calculated by means of the following equation:

$$\sigma_{tot} = \frac{t}{R_{tot} \cdot S} \tag{1}$$

where t refers to the sample thickness and S is the surface area. Activation energies, E_a, were calculated from the cooling process spectra (from $\sim$85 °C to 30 °C at the end of the CSP), following the same procedure used in ref. 20. The cooling spectra of the 20@H₂O sample are shown as an example in Fig. 3. The cold-sintered samples were characterized by XRD (Advance diffractometer, Bruker Theta-Theta, Germany), between 5 and 90 degrees and SEM (FEG-SEM Quanta 200F) to study the changes that occurred at the microstructural level.

Results and discussion

The normalized impedance spectra at 30 °C after the CSP, when no pressure is applied, are shown in Fig. 4 for the four tested samples together with the equivalent circuit used for the fitting. The values of the fitted spectra can be seen in Tables S2–S5 of the ESI,† where the last row in italics refers to the measurement without pressure. It can be observed how the 20@solid sample, prepared just by mixing the solids, has a resistance three or more times higher than the other samples. All the results are summarized in Table 3, where the activation energies are obtained from the Arrhenius plot shown in Fig. 5.

Sample 20@solids shows that mechanical mixing of the salts LiNO₃ and LiOH with LATP leads to a non-homogeneous powder mixture, which worsens both the total ionic conductivity and activation energy, 9.66×10^{-6} S cm⁻¹ and 0.595 eV, respectively. For the 20@no-H₂O sample, the ionic conductivity is higher than in the previous one and the activation energy is lower: 7.03×10^{-5} S cm⁻¹ and 0.358 eV, respectively. Despite the absence of water as the homogenizing agent, a previous mixing of both lithium chemicals (20@no-H₂O) enhances the final properties when compared with the simultaneous mixing of raw lithium chemicals (20@solids). Both values are similar
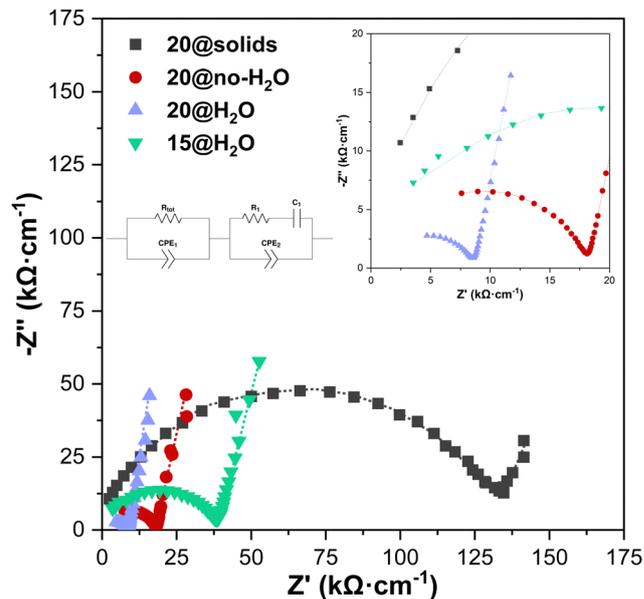

Fig. 4 Normalized impedance spectra of the samples studied (symbols for experimental points and dotted line for the fitting).

Table 3 Ionic conductivities of the different samples studied at 30 °C

Sample	R_{tot} (kΩ)	t (mm)	σ_{tot} (S cm⁻¹)	E_a (eV)
20@solids	14.885	1.10	9.66×10^{-6}	0.595 ± 0.010
20@no-H₂O	2.267	1.22	7.03×10^{-5}	0.358 ± 0.003
20@H₂O	0.875	1.01	1.51×10^{-4}	0.366 ± 0.005
15@H₂O	4.664	1.20	3.36×10^{-5}	0.434 ± 0.005

to those obtained by the authors when sintering the same LATP using a 3M acetic acid solution as the TLP instead of the eutectic LiNO₃ : LiOH (6.90×10^{-5} S cm⁻¹ and 0.363 eV[19]).

Sample 20@H₂O reveals the effect of water addition in a better homogenization process leading to a superior ionic conductivity (1.51×10^{-4} S cm⁻¹) and an activation energy of 0.366 eV. This ionic conductivity is 2.2 times higher than that obtained with LATP cold-sintered using 3M acetic acid solution as the TLP [17]. Reducing the hydroflux content to 15 wt% (sample 15@H₂O) results in the worsening of properties, although they are still competitive (ionic conductivity of 3.36×10^{-5} S cm⁻¹ and activation energy of 0.434 eV). The increase of $\sim$20% in the activation energy reflects that a better homogenization process reduces the energetic barrier of the intergranular phase.

It should be emphasized that samples of LATP containing the hydroflux with appropriate processing prior to the CSP (*i.e.*, samples 15@H₂O and particularly 20@H₂O):

(a) Have better ionic conductivity after the CSP than the same cold-sintered LATP with 3M acetic acid solution as the TLP, which means that the intergranular phase presents a lower energy barrier in terms of lithium-ion diffusion.

(b) Require lower demanding sintering conditions in terms of pressure (400 MPa) than the same cold-sintered LATP with 3M acetic acid solution as the TLP (700 MPa).
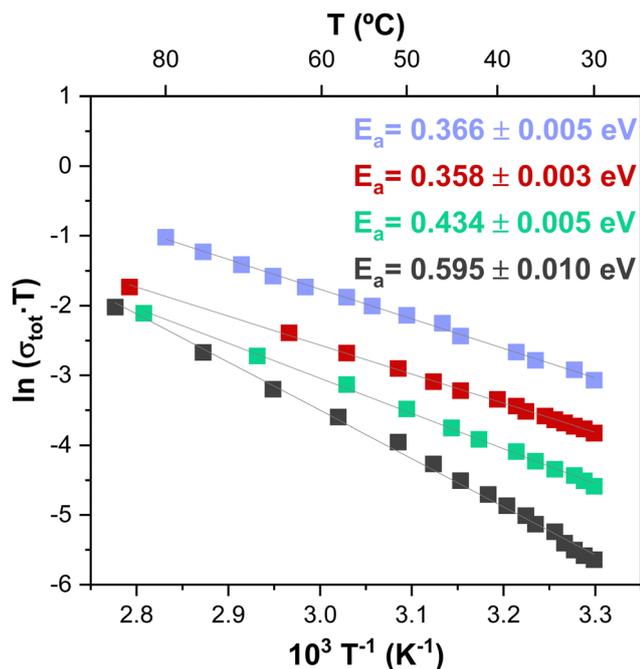
Fig. 5 Arrhenius plot of the tested samples. The grey squares refer to 20@solids, the red ones to 20@no-H$_2$O, the blue ones to 20@H$_2$O and the green ones to 15@H$_2$O.

Fig. 6 XRD spectra of the different compositions analyzed.

(c) Have better ionic conductivity than other LATP samples obtained *via* the CSP reported in the literature (see Table S6, ESI†). Some of these samples have undergone a post-annealing treatment.

The results demonstrate the positive impact of using a hydroflux as a TLP in the CSP on the ionic conductivity and its relevance towards the enhancement of the CSP.

Samples were analysed by XRD, and the spectra are shown in Fig. 6. It can be observed that when eutectic mixtures were introduced into the CSP, no new peaks appeared with respect to the pure LATP (ICSD 14585), suggesting that eutectic forms a glassy phase that persists when cooling after sintering.

Fig. 7 shows the SEM images of the general microstructure for the tested samples. Two different behaviours can be observed: (i) for samples 20@solids and 20@no-H$_2$O (Fig. 7(a) and (b)) the microstructure is heterogeneous, with pores denoting a poor sintering process, corresponding to a poor initial homogenization stage during sample preparation. Typically, the porosity leads to non-optimal properties in terms of ionic conductivity and/or activation energy; (ii) for samples 15@H$_2$O and 20@H$_2$O (Fig. 7(c) and (d)), the microstructure is markedly different. There is a homogeneous microstructure aimed by two factors, the introduction of the hydroflux in an appropriate amount and the use of water to better distribute the hydroflux around the LATP particles of the sample.

For a better understanding, higher magnification images are shown in Fig. 8. These images show an improvement in the microstructure due to the effect of the hydroflux preparation and the addition of water as a homogenization agent in sample preparation. For the 20@solids sample (Fig. 8(a)), a non-homogeneous and
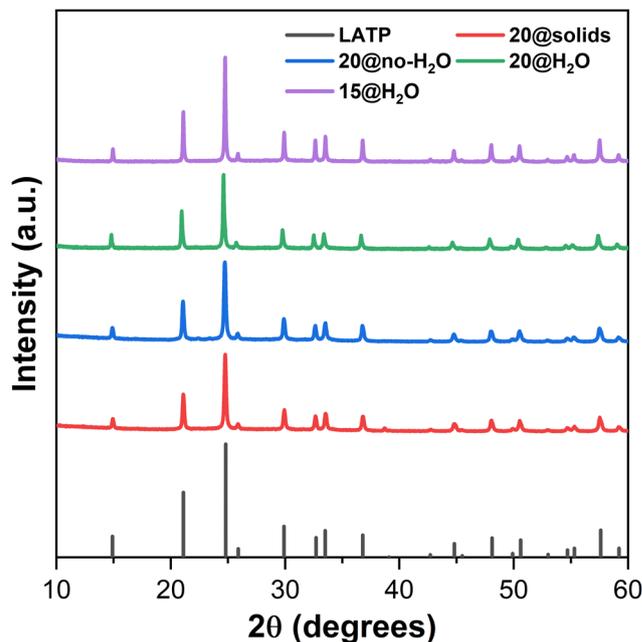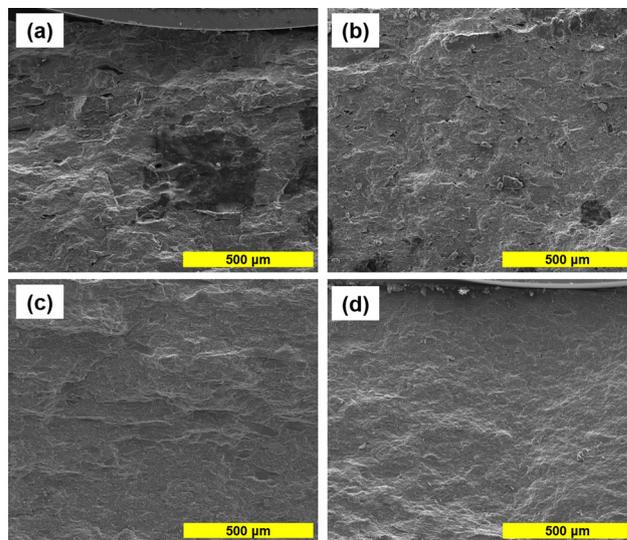

Fig. 7 SEM images of the general microstructure of the tested samples: (a) 20@solids, (b) 20@no-H$_2$O, (c) 15@H$_2$O and (d) 20@H$_2$O.

discontinuous glassy phase appear over some LATP particles, proving that the hydroflux is in concentrated areas, justifying the poor densification due to its weak distribution. Fig. 8(b) shows the 20@no-H$_2$O sample where hydroflux particles can be seen, different in shape from the LATP ones, reiterating the same behaviour as in the 20@solids sample, leading to a poor densification. To confirm this, an EDS mapping was carried out to identify if these particles correspond to the hydroflux. The results are shown in Fig. 9, where it can be seen that the contents of O and N are enhanced at these points due to the presence of LiOH and LiNO$_3$, and the energy spectrum
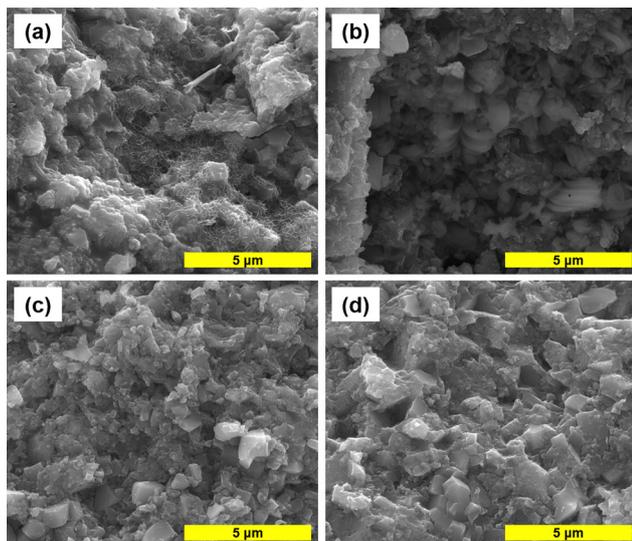
Materials Advances

Fig. 8   SEM images showing the distribution of the hydroflux along the microstructure of samples prepared (a) 20@solids, (b) 20@no-H$_2$O, (c) 15@H$_2$O and (d) 20@H$_2$O.

shows a peak corresponding to N. All these corroborate the previous discussion. The microstructures of 15@H$_2$O and 20@H$_2$O (Fig. 8(c) and (d)) show no clear difference between them. In both cases, the hydroflux is uniformly distributed, pointing out the influence of the use of water to enhance the homogenization of the hydroflux in the LATP and promote densification. The different hydroflux content of the 15@H$_2$O and 20@H$_2$O samples is responsible for obtaining such a high ionic conductivity for the 20@H$_2$O sample, making it the optimal composition under these CSP conditions.

Conclusions

In this work, the effect of hydroflux addition as a TLP for the CSP was validated. The hydroflux consisted of a eutectic mixture of LiNO$_3$:LiOH in a molar ratio of 60:40 added to LATP, with and without water as a homogenizing agent. The effect of hydroflux addition resulted in an increase in the total ionic conductivity of up to 1.51×10^{-4} S cm^{-1} and an activation energy of 0.366 eV for the sample prepared at 400 MPa, 200 °C and 90 minutes of sintering time with 20 wt% of hydroflux. SEM images have demonstrated the necessity of water to initially disperse the hydroflux and obtain a well homogenized microstructure, as it has been pointed out to be a crucial step.

Author contributions

Andrés Mormeneo-Segarra: investigation, validation, and writing – original draft. Sergio Ferrer-Nicomedes: investigation, validation, and writing – original draft. Nuria Vicente-Agut: supervision and writing – review & editing. Antonio Barba-Juan: supervision, and writing – review & editing.

Data availability

The data supporting the results of this study are currently available from the corresponding author, N. V.-A., upon reasonable request.

Conflicts of interest

There are no conflicts to declare.

Acknowledgements

References

1 T. Wang, W. Luo and Y. Huang, *Acc. Chem. Res.*, 2023, **56**, 667–676.

2 W. Zhang, V. Koverga, S. Liu, J. Zhou, J. Wang, P. Bai, S. Tan, N. K. Dandu, Z. Wang, F. Chen, J. Xia, H. Wan, X. Zhang, H. Yang, B. L. Lucht, A.-M. Li, X.-Q. Yang, E. Hu, S. R. Raghavan, A. T. Ngo and C. Wang, *Nat. Energy*, 2024, **9**, 386–400.

3 T. Wang, J. Duan, B. Zhang, W. Luo, X. Ji, H. Xu, Y. Huang, L. Huang, Z. Song, J. Wen, C. Wang, Y. Huang and J. B. Goodenough, *Energy Environ. Sci.*, 2022, **15**, 1325–1333.

4 J. Janek and W. G. Zeier, *Nat. Energy*, 2023, **8**, 230–240.

5 Q. Zhao, S. Stalin, C.-Z. Zhao and L. A. Archer, *Nat. Rev. Mater.*, 2020, **5**, 229–252.

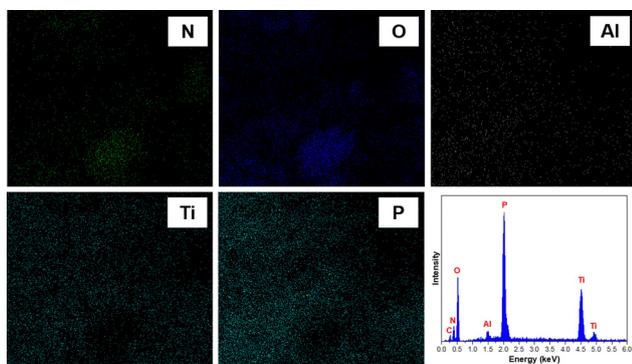6 W. Xiao, J. Wang, L. Fan, J. Zhang and X. Li, *Energy Storage Mater.*, 2019, **19**, 379–400.

Fig. 9   EDS mapping of the 20@no-H$_2$O sample showing the most representative elements present and their energy spectra.

7 J. G. Guo Hanzheng, A. Baker, M. T. Lanagan, E. R. Kupp, G. L. Messing and C. A. Randall, *Angew. Chem., Int. Ed.*, 2016, **55**, 11457–11461.

8 H. Guo, A. Baker, J. Guo and C. A. Randall, *ACS Nano.*, 2016, **10**, 10606–10614.

9 A. Galotta and V. M. Sglavo, *J. Eur. Ceram. Soc.*, 2021, **41**, 1–17.

10 K. Takashima, Y. Iwazaki and C. A. Randall, *Jpn J. Appl. Phys.*, 2021, **60**, 126505.

11 R. D. Floyd, S. Lowum and J. P. Maria, *J. Mater. Sci.*, 2020, **55**, 15117–15129.

12 S. Lowum, R. Floyd and J.-P. Maria, *J. Mater. Sci.*, 2020, **55**, 12747–12760.

13 K. Tsuji, A. Ndayishimiye, S. Lowum, R. Floyd, K. Wang, M. Wetherington, J. P. Maria and C. A. Randall, *J. Eur. Ceram. Soc.*, 2020, **40**, 1280–1284.

14 K. Tsuji, Z. Fan, S. H. Bang, S. Dursun, S. Trolier-Mckinstry and C. A. Randall, *J. Eur. Ceram. Soc.*, 2022, **42**, 105–111.

15 K. Nakagawa, M. Iwasaki, Z. Fan, J. I. Roscow and C. A. Randall, *J. Eur. Ceram. Soc.*, 2023, **43**, 4015–4020.

16 A. Mormeneo-Segarra, S. Ferrer-Nicomedes, N. Vicente-Agut and A. Barba-Juan, *Ceram. Int.*, 2023, **49**, 36497–36506.

17 Collection of Phase Diagrams, **https://www.crct.polymtl.ca/fact/phase_diagram.php?** file = LiNO$_3$-LiOH.jpg&dir = FTsalt, (accessed 22 January 2024).

18 A. Mormeneo-Segarra, S. Ferrer-Nicomedes, S. Simon, N. Vicente-Agut, J. C. Jarque-Fonfría and A. Barba-Juan, *Solid State Ion*, 2024, **406**, 116482.

19 A. Mormeneo-Segarra, S. Ferrer-Nicomedes, N. Vicente-Agut and A. Barba-Juan, *J. Eur. Ceram. Soc.*, 2024, **44**, 5105–5114.

20 S. Ferrer-Nicomedes, A. Mormeneo-Segarra, N. Vicente-Agut and A. Barba-Juan, *J. Power Sources*, 2023, **581**, 233494.